Microelectronics Reliability 87 (2018) 113–124

Contents lists available at ScienceDirect

Microelectronics Reliability

journal homepage: www.elsevier.com/locate/microrel

Sensor system optimization to meet reliability targets

Wolfgang Granig[a,*], Lisa-Marie Faller[b], Hubert Zangl[b]

[a] Infineon Technologies Austria AG, Siemensstrasse 2, Villach 9500, Austria
[b] Alpen Adria Universitaet, Universitaetsstrasse 65-67, Klagenfurt 9020, Austria

ARTICLE INFO

Keywords:
Sensor optimization
Sensor reliability
Optimal design
Safety

ABSTRACT

In this work, we show the influence of sensor system measurement uncertainties to sensor system reliability and ways to meet reliability targets. A general model to handle measurement uncertainties is defined and the according influence to reliability is presented, which is defined as probability of meeting specification requirements. Initial step is to optimize sensor systems concerning lowest influences of sensor system parameter fluctuations to the measurement uncertainty using statistical optimization methodologies. In case the influence of unknown nuisance parameters cannot be sufficiently suppressed, such parameters may be additionally measured in order to further reduce measurement uncertainties. The remaining uncertainties are again addressed using statistical optimization methodologies. Finally, measurement uncertainty also affects the reliability of such a system. For sensor systems in safety critical applications it may thus be required to include measures such as redundancy. This is also included in the investigations. Further examples for explained optimization methodologies of measurement uncertainty reduction are presented.

1. Introduction

Our modern world is fully digitized: starting from consumer goods such as mobile phones, TVs and body scales, going to vehicles such as cars, airplanes and trains to automated production lines based on human-robot-interaction. All of these electronic devices need a way to interface to the real, physical world: commonly, sensor systems present a way to realize this interfacing. These sensor systems present the means for electronic systems to comprehend their environment. Depending on the application, it is more or less important that this comprehension is truthful and dependable. As soon as a physical quantity of interest and its representation (analog or digital) from sensor systems differ too much in value, this is either useless – in case of the smart watch which does not reliably sense our heart frequency – or dangerous in case of the accelerometer which is in charge of the airbag control. Sensor system reliability is thus a major concern, not only in terms of customer satisfaction, but also for safety reasons. In this work, we consequently present means to define and quantize reliability by introducing a general mathematical model. Ways to improve the sensor systems' reliability are presented: one way is to use optimization methods of the existing systems using statistic optimization techniques [1], another way is to additionally measure known, correlated disturbing influences and compensate those [2, 3], and also a combination of both approaches is possible. Where the effort is justified by the application, redundancy can be a way to improve the sensor system reliability, especially for safety requirements. The latter is often the case in standardized safety related automotive applications [4].

1.1. Sensor system definition

A general abstraction of a sensor system is illustrated in Fig. 1. Here θ is the physical quantity of interest. Depending on the employed sensor effect, this is further converted into the electrical domain by the sensor front-end or subsequent circuitry. It is now an (analog or digital) electrical quantity and represented by the Random Variable (RV) Y. A RV basically is a function which, besides possible deterministic variables, also depends on random, i.e. unknown, inputs. In system theory, such functions, which describe the way of how a system acts on a quantity of interest, are often also called transfer-functions. Here, it is assumed that Y depends on systematic influences (bias-voltage, calibration-parameters, stress etc.) [2, 3] as well as random influences (noise, Electro Magnetic Interference (EMI) etc.) introduced by the sensor front-end and/or respective circuitry. To reconstruct the physical quantity from the electrical representation Y, a mapping function as part of the digital signal processing is necessary. This mapping function is termed an *estimator* for the physical quantity of interest and its sensor system output value is often denoted as $\hat{\theta}$ to indicate the relation to the true physical quantity of interest (θ). This estimation even can be performed inside the sensor system with electrical output values interpreted in the same physical quantity as θ [1].

* Corresponding author.
E-mail address: wolfgang.granig@infineon.com (W. Granig).

https://doi.org/10.1016/j.microrel.2018.06.005
Received 31 January 2018; Received in revised form 16 May 2018; Accepted 6 June 2018
Available online 15 June 2018

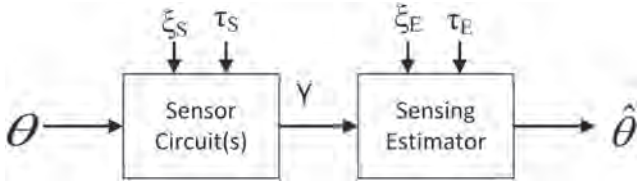

Fig. 1. General block diagram of a sensor system with transfer of a physical quantity θ into electrical signals Y with estimation to an interpretable output value M to get an interpreted estimation of the real value $\hat{\theta}$.

1.2. Sensor system deviations

The way to express measurement uncertainty and methods to mathematically deal with them are defined in the *Guide to the expression of uncertainty* [5] and respective supplements. For existing sensor systems, the tolerable uncertainties and deviations are limited by specifications. When a new sensor system is implemented, these specifications are the design criteria for sensor system optimization. As explained before and compare Eq. (1) the sensor circuit output value Y (or output vector Y) depends on systematic parameters, now termed ξ, and random terms, which we now call τ. In terms of transfer-functions, we can split it into the ideal transfer-function $h(\cdot)$ and the deviation transfer-function $e(\cdot)$. From measurements, Y an estimation of θ called $\hat{\theta}$ can be found via $u(\cdot)$ by Eq. (2). The final deviation in Eq. (3) is the difference between sensor output and ideal value.

$$Y = h(\theta, \xi) + e(\theta, \xi, \tau) \tag{1}$$

$$\hat{\theta} = u(Y, \xi, \tau) \tag{2}$$

$$\Delta = \hat{\theta} - \theta \tag{3}$$

Some of the most common sources of measurement uncertainties and deviations are:

- Noise (thermal, quantization)
- Production (spread)
- Influencing parameters (temperature, stress)
- Calibration (calibration deviation/quantization)
- Lifetime drifts (aging)
- External sources of deviation (Strayfields, EMI)
- Sensor system faults

1.3. Definition of reliability and unreliability

The reliability of a sensor system acc. [6] is defined as the *ability of a product to perform a required function at or below a stated failure rate for a given period of time*. We further define the *required function* as correctly providing measurement results within the specification limits at specified conditions (e.g.: temperature, supply-voltage, lifetime). In engineering, a more often used term is unreliability which is the probability of a sensor system providing measurement value outside the specification (failures). Several standards are available dealing with reliability or unreliability (eg.: Ref. [7]) or at least to verify them in automotive [8], industrial [9] and general dependability standards [10]. In this work, we consider measurement uncertainty as Gaussian distributed deviations of the sensor output value $\hat{\theta}$ from the ideal output value θ according Eq. (3). Since we assume Gaussian distributions of measurement deviations with average deviation μ and variance σ^2 according to the general definition of the respective probability density function (pdf) shown in Eq. (4) there is always a probability larger than zero to violate specification limits, mathematically because of the infinite spread Gaussian distribution. In this work we assume hardware-faults as Gaussian distribution with larger and unknown variance. As the variance of deviations caused by faults is unknown, we consider the worst case. In practical setting, a maximum

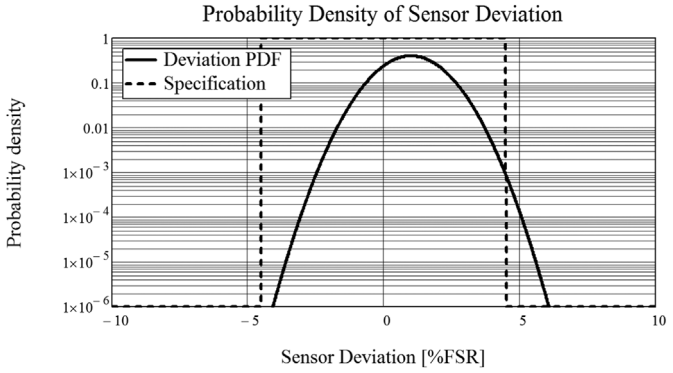

Fig. 2. Gaussian distribution of all present measurement uncertainties shown together with specification limits in logarithmic scale.

number of specification limit violations are allowed and measured as probability in % or parts per million (ppm). An example with sensor deviations in % of measurement full-scale-range (%FSR) acc. [11] comprising statistical and systematic deviations is shown in Fig. 2.

$$pdf(\Delta) = \frac{1}{\sqrt{2\pi}\sigma} e^{-\frac{1}{2}\left(\frac{(\Delta-\mu}{\sigma}\right)^2}. \tag{4}$$

Unreliability in this sense is the integral of all probability densities outside the minimum and maximum specification limits $\pm \Delta_{spec}$. Mathematically it can be written as shown in Eq. (5). This unreliability or probability of specification violation is dependent on mean-value and variance of this modeled Gaussian distribution. These probabilities can be determined relative to the specification limit according Fig. 3.

$$P_{fail}(|\Delta| > \Delta_{spec}) = \int_{-\infty}^{-\Delta_{spec}} pdf(\Delta) + \int_{+\Delta_{spec}}^{+\infty} pdf(\Delta). \tag{5}$$

2. Sensor system optimization methods

We want to optimize the sensor output concerning reliability to provide sensor output values within specification limits. In general, this optimization criterion can be defined by $\psi(\cdot)$, which depends on the input variable θ and the design parameters ξ. Since θ is given, only the

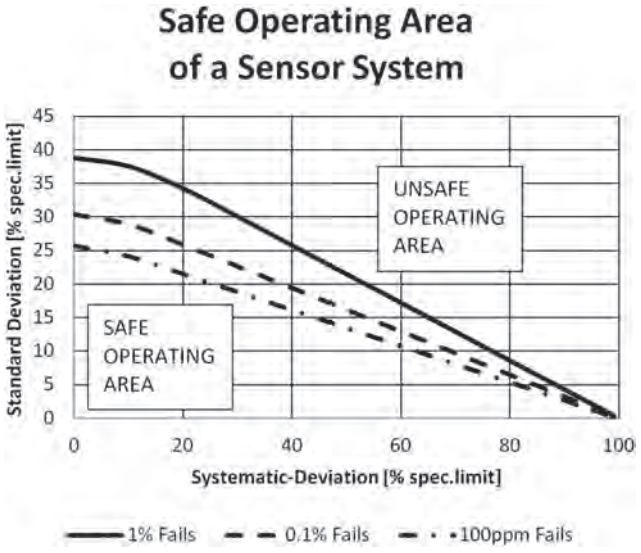

Fig. 3. This graph shows the safe/unsafe operating area (SOA) of a sensor system providing data within specification limits and assuming Gaussian distribution of deviations with parameters mean and standard-deviation. These parameters are scaled in % relative to the specification limit and thus are valid for all possible limits.

design parameters ξ can be used for optimization, optimal parameters can be found by Eq. (6).

$$\xi^* = \arg\min_{\xi\in\Xi} \psi(\theta, \xi) \tag{6}$$

$$\xi = \{\xi_G, \xi_P, \xi_Y, \xi_E\} \tag{7}$$

$$\tau = \{\tau_G, \tau_P, \tau_Y, \tau_E\}. \tag{8}$$

Systematic design parameters ξ contain contributions of different sources shown in Eq. (7), where G represents geometric parameters, P material parameters, Y sensor circuit parameters and E estimator configuration parameters. Nuisance parameters τ contain contributions of the same sources shown in Eq. (8).

$$E\{\tau\} = 0 \tag{9}$$

$$cov\{\tau\} = E\{\tau\tau^T\}. \tag{10}$$

The nuisance-parameters are zero mean shown in Eq. (9) and contain a certain covariance according Eq. (10).

We can apply now following different methods to find these optimized sensor system parameters:

2.1. Sensor system optimization using statistical methods

When disturbing influences are not known beforehand and the effort to determine possible correlations is difficult or even infeasible (e.g. fabrication process is not well-studied), one way to reduce the influence of these deviations is by design optimization. System parameters can be shifted to optimum values as shown in Fig. 4 according to Eq. (6), where the spread of influencing parameters have lowest influence to the optimization criterion, which is the case for optimal-point B in this figure. Several methods from optimal design of experiments and their optimality criteria can be used to minimize the effect of influencing parameters.

Various statistical optimization methodologies are described in related literature, such as Refs.[1, 12, 13] and [14]. Basically, we can distinguish on one hand between optimizations where the Fisher-Information (or the inverse of it) is used, and on the other hand Bayesian principles.

2.1.1. Fisher information based optimization

The design parameter vector ξ comprises all information describing the configuration, such as the sensor location, measurement reference, and transfer-characteristics. The aim is to find the configuration ξ^* that minimizes the probability of output value change by additional measurement values. The amount of information about the variable of interest which is contained in the observed variable is called the Fisher information I. The inverse of the Fisher information I^{-1} is also called

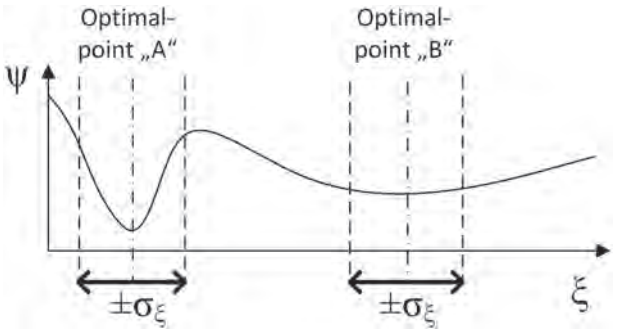

Fig. 4. Optimization of sensor systems with uncertainties also consider the statistical spread of influencing parameters ξ to the optimization criteria ψ. Optimum point B in this figure leads to lower spread than Optimum A, however the peak optimum point is less accurate, but it does not consider the real world unavoidable spread of influencing parameters.

dispersion D defined by Eq. (11)

$$D = I^{-1} \tag{11}$$

and represents a lower bound for the variance of any unbiased estimator for the parameter in question, see Eq. (12).

$$var(\hat{\theta}) \geq \frac{1}{I(\theta, \xi)}. \tag{12}$$

The Fisher information I in this sensor system is given by Eq. (13):

$$I(\theta, \xi) = -E\left\{\frac{\partial^2 ln(p(x; \theta, \xi))}{\partial\theta^2}\right\} \tag{13}$$

The optimal design configuration ξ^* can be found by Eq. (14) where H represents the possible design space.

$$\xi^* = \arg\min_{\xi\in H} D(\theta, \xi) \tag{14}$$

In case of linear models where the transfer-function can be treated independent of input parameters, a Minimum Variance Unbiased Estimation (MVUE) of transfer-characteristics defined by Eq. (15) can be applied.

$$Y = h(\xi)\cdot\theta + w. \tag{15}$$

There, w represents Additive White Gaussian Noise (AWGN) and all random influences are gathered in this noise-term. The Fisher information then can be gathered by Eq. (16) to get estimated physical quantities by Eq. (17) and further optimized sensor system parameters by Eq. (18).

$$I = \frac{h(\xi)^T\cdot h(\xi)}{\sigma} \tag{16}$$

$$\hat{\theta} = [h(\xi)^T\cdot h(\xi)]^{-1}\cdot h(\xi)^T\cdot Y \tag{17}$$

$$\xi^* = \arg\min_{\xi\in H} |D(\xi)| = \arg\min_{\xi\in H} |[h(\xi)^T\cdot h(\xi)]^{-1}|. \tag{18}$$

There, ξ^* represent the optimal parameters for ξ according D-optimality criterion.

In the general, Gaussian case according Eq. (19)

$$Y = h(\theta, \xi) + w \tag{19}$$

the uncertainty of measurements can be modeled using jointly Gaussian distribution with certain variances expressed in the covariance-matrix C, the Fisher information can be obtained from Eqs. (20) and (21) according [1].

$$[I(\theta, \xi)]_{ij} = \left(\frac{\partial h(\theta, \xi)}{\partial\theta_i}\right)^T C^{-1}(\theta, \xi)\left(\frac{\partial h(\theta, \xi)}{\partial\theta_j}\right) + \tag{20}$$

$$+ \frac{1}{2} tr\left(C^{-1}(\theta, \xi)\frac{\partial C(\theta, \xi)}{\partial\theta_i}C^{-1}(\theta, \xi)\frac{\partial C(\theta, \xi)}{\partial\theta_j}\right). \tag{21}$$

Several criteria using the inverse of the Fisher information called dispersion D shown in Eq. (11) to optimize the influence of design parameters are available: The most common target is the D-criterion which uses the determinant of the dispersion matrix, see Eq. (22).

$$\Psi_D(\theta, \xi) = \max_{\theta\in\Theta} |D(\theta, \xi)|. \tag{22}$$

Other optimization criteria based on the dispersion matrix use the trace (A-criterion) or the eigenvalues (E-criterion) of D. These criteria however assume unbiased and optimal estimators.

2.1.2. Bayesian optimization methodologies

Often, we do not know about design-parameter uncertainties, but we roughly know properties of their distributions such as the mean and variance (i.e. tolerances given by the manufacturer). Having such information at hand, together with the knowledge of distributions of the parameter to be estimated, this allows to construct a Bayesian mean

square error estimator. Estimators based on the Bayesian approach allow the consideration of prior knowledge. Many estimators may exist, which are optimal with respect to a certain point of the design, but the Bayesian methodology will yield an estimator which results in the best *on average* for the entire domain [1]. Such an estimator is found by minimizing the mean square error (MSE) or Bayesian Mean Square Error (BMSE). Optimization applying the Bayesian mean square error are done according Eqs. (23), (24) and (25).

$$BMSE([\hat{\theta}]_i) = E\{(\theta_i - \hat{\theta}_i)^2\} \tag{23}$$

$$BMSE([\hat{\theta}]_i) = \int\int (\theta_i - \hat{\theta}_i)^2 p(y, \theta_i) d\theta_i dy \tag{24}$$

$$\hat{\theta} = \int \theta p(\theta|y) d\theta = E\{\theta|y\}. \tag{25}$$

In classical approaches, all deterministic parameters are taken into account. Particularly, this means a necessity to consider the nuisance parameters as well since they are considered deterministic. Here, and this motivates the Bayesian approach, it is possible to exclude the nuisance parameters by integration over their pdfs [1]. While analytic computations of integrals may be cumbersome, we exploit properties of the employed Design Of Experiments (DOE) to implement this. To approximate the true deterministic dependence ($h(\cdot)$ in Eq. (1)), the so-called forward problem is solved by generating a system model from simulation/measurement data. In case of linear estimation, the expectation of the posterior distribution can be obtained using the Bayesian Linear Minimum Mean Square Estimation (BLMMSE). In general of Minimum Mean Square Error (MMSE), we define Eq. (26).

$$\hat{\theta} = E\{\theta|y\}. \tag{26}$$

In case of linear estimations, we can assume a linear relationship in Eq. (27)

$$E\{\theta|y\} = Wy + B \tag{27}$$

with linear terms defined in Eq. (28)

$$W = C_{\theta Y} C_{YY}^{-1} \tag{28}$$

and bias defined in Eq. (29)

$$B = \overline{\theta} - W\overline{y} \tag{29}$$

where $C_{\theta Y}$ and $C_{Y\ Y}$ are covariance matrices of the estimate and the measurement, and of the individual measurements respectively, accounting also for the measurement noise. $\overline{\theta}$ is used to denote the expected value of the parameters to be estimated with respect to their prior distributions. Correspondingly, $\overline{y}$ means the expected value of the measurement.

In cases where we cannot or do not want to use an unbiased estimator, we can operate on the Mean Square Error (MSE) criterion. In Ref. [13], the MSE-matrix $R(\xi)$ was defined as

$$R(\theta, \xi) = E\{(\hat{\theta} - \theta)(\hat{\theta} - \theta)^T\} \tag{30}$$

where the estimator is chosen as

$$\hat{\theta} = \theta + \hat{\theta}_b(\theta, \xi) + \hat{\theta}_n(\theta, \xi) \tag{31}$$

with $\hat{\theta}_b$ as bias error and $\hat{\theta}_n$ the random error term. This results in the MSE-matrix

$$R(\theta, \xi) = \hat{\theta}_b(\theta, \xi)\hat{\theta}_b^T(\theta, \xi) + cov[\hat{\theta}_n(\theta, \xi)]. \tag{32}$$

Then, the same optimization criteria as for the dispersion can be used. In this case, the D_R criterion is given by Eq. (33)

$$\Psi_{D_R} = \max_{\theta \in \Theta} |R(\theta, \xi)|. \tag{33}$$

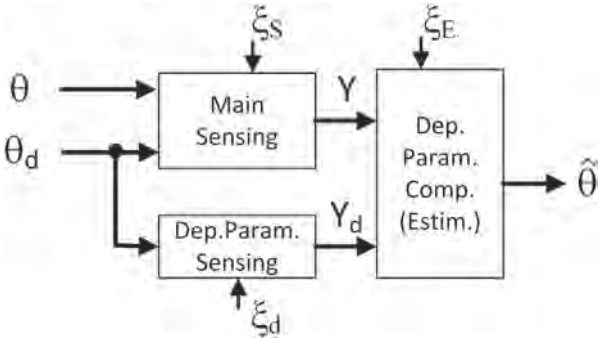

Fig. 5. Block diagram of a sensor system with additional measurement of dependent influencing parameter θ_d and according compensation in the succeeding estimator.

2.2. Sensor system optimization considering dependent parameters

In case of all statistical optimizations are not sufficient to provide sensor systems fulfilling the reliability requirement further improvements to the sensor system have to be found. One well known way is to analyze correlations of the measurement error Δ with influencing parameters. There following parameters are influencing correctly estimating measurement output values, which are handled differently:

- Temperature, stress, air pressure etc.
- External interference (strayfield, EMC)
- Lifetime drifts

2.2.1. Sensor system optimization by dependent parameter compensation

The make use of correlations to influencing parameters is the most often used principle to reduce the sensor output uncertainty. In this case the dependent physical parameters (like temperature, mechanical stress, and air pressure) are measured in parallel to the sensing quantity. When using block diagram of Fig. 1 then the measurement quantity θ becomes a vector containing the desired measurement quantity and the dependent parameter θ_d (see Fig. 5). The dependent parameter compensation is performed in the succeeding estimator using mainly polynomial compensation algorithms including dependent offset compensation using the influencing parameter information matrix H_d shown in Eq. (34). There the noise-terms are not considered because we assume them zero mean and not part of the compensation.

$$\hat{\theta}(Y, Y_d) = Y \cdot H_d(Y_d) \cdot \xi_{E_G} + H_d(Y_d) \cdot \xi_{E_O}. \tag{34}$$

Here, the dependent parameters for the gain compensation of the estimator are represented in ξ_{E_G} and the offset related compensation parameters of the estimator are denoted in ξ_{E_O}. An example of second order compensation for each measurement sample i is shown in Eq. (35).

$$\hat{\theta}_i = Y_i \cdot [1 \quad Y_{d_i} \quad Y_{d_i}^2] \begin{bmatrix} \xi_{E_{G0}} \\ \xi_{E_{G1}} \\ \xi_{E_{G2}} \end{bmatrix} + [1 \quad Y_{d_i} \quad Y_{d_i}^2] \begin{bmatrix} \xi_{E_{O0}} \\ \xi_{E_{O1}} \\ \xi_{E_{O2}} \end{bmatrix}. \tag{35}$$

One of the challenging aspects of dependent parameter compensation is the calibration after sensor system production. The calibration equipment uncertainty directly influences the uncertainty of the final sensor system to optimize. Basically, the same estimation principles of finding the minimum variance estimation as for the measurement values are used to get compensation parameters ξ_{E_G} and ξ_{E_O}. To apply this, we define the matrix H_d based on measurement values according Eqs. (36) and (37), which is done during productive calibration of this sensor system.

$$H_d = \begin{bmatrix} 1 & Y_{d_1} & Y_{d_1}^2 \\ \vdots & \vdots & \vdots \\ 1 & Y_{d_i} & Y_{d_i}^2 \end{bmatrix} \tag{36}$$

$$Y = \begin{bmatrix} Y_1 \\ \vdots \\ Y_i \end{bmatrix}. \tag{37}$$

The bias (offset) as well as gain values can be found by first merging Eqs. (36) and (37) into Eq. (38). Then, Eq. (39) can be applied to get estimator offset ($\xi_E O$) and gain ($\xi_E G$) parameters.

$$H_{d2} = \begin{bmatrix} H_d \\ H_d \cdot Y \end{bmatrix} \tag{38}$$

$$\begin{bmatrix} \xi_{E_O} \\ \xi_{E_G} \end{bmatrix} = (H_{d2}^T \cdot H_{d2})^{-1} \cdot H_{d2}^T \cdot \theta. \tag{39}$$

2.2.2. Lifetime drifts

Lifetime drifts are most critical deviations because they are hardly compensable. Every electrical/electronic circuit suffers from lifetime drifts of electrical parameters. These drifts cause lifetime-dependent deviations from the target output value, sometimes even with systematic deviation contributions and not reliably predictable. In this paper we only consider lifetime-drifts as additional uncertainty which has to be considered for the rest of the system parameters to optimize, especially for calibration and qualification. There, we need to consider systematical and statistical lifetime-drifts, an example can be seen in Fig. 6.

Today sensors for reliable systems like industry, automotive and aerospace are qualified by certain accelerated aging stress tests defined in Refs.[8, 9]. Additionally, several worst-case operating conditions are defined for this accelerated lifetime test. Some examples are:

- HTOL (High Temperature Operating Lifetime)
- HTS (High Temperature Storage)
- TC (Temperature Cycling)

A practical way to handle lifetime-drifts is to reduce their effects generated mainly by the transfer-function of the sensor-elements according Eq. (1). Here, previous explained statistical optimization methods are most useful, especially when a systematic lifetime drift can be predicted [15] or modeled as shown in Ref. [16]. In case it would be possible to measure lifetime-degradation, one can even define a system with influencing parameter measurement and compensation of this lifetime-effect proposed by Ref. [17].

2.3. Sensor system optimization considering test- and qualification-equipment

In case of best possible deterministic and statistic optimized sensor system, there always remain uncertainties initiated by the calibration

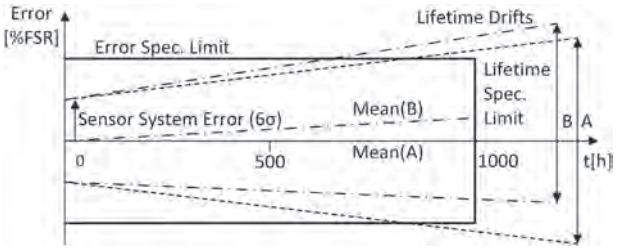

Fig. 6. Lifetime-drifts of measurement uncertainties can increase symmetrically (case A) or additional systematic lifetime-drifts can occur (case B) resulting in an unsymmetric measurement uncertainty after the target lifetime.

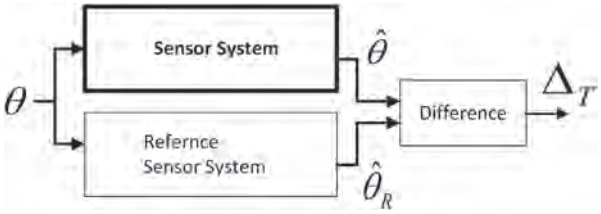

Fig. 7. This block diagram shows a configuration during sensor system calibration or verification. The difference of the system under test and the reference sensor system is a measure of uncertainty for the sensor system under test.

and verification-equipment (see Fig. 7). When comparing a sensor output value with a reference sensor value this is a subtraction of both values as shown in Eq. (40).

$$\Delta_T(\theta, \xi) = \hat{\theta}(\theta, \xi) - \hat{\theta}_R(\theta). \tag{40}$$

Since we are not able to compare the desired sensor system with the real value and we use an other sensor system as reference instead generates additional sources of uncertainty. To analyze the remaining uncertainty we only need to take Δ_T as additive compensation value to $\hat{\theta}$ to get the corrected value $\hat{\theta}_{corr}$ which results in uncertainties defined by the reference value shown in Eq. (41).

$$\hat{\theta}_{corr} = \hat{\theta} - \Delta_T = \hat{\theta} - (\hat{\theta} - \hat{\theta}_R) = \hat{\theta}_R. \tag{41}$$

This shows us the influence of reference-sensor uncertainties during production-test and productive calibration as well as verification of qualification test results for sensor system optimizations. It is physically not possible to get a better performing system than the reference system performance used for calibration, test of production and qualification. To get a full picture of extracting the probability of passing a qualification test is shown in Fig. 8. In this picture, one can also easily recognize, that the reference measurement uncertainty has a significant influence to the probability of specification limit violations without detection. High uncertainties will increase the probability of sensor system specification violations. High uncertainties also lead to an increased probability of wrong detected specification violations. The calculation of probability $Pv1$,$Pv2$,$Pd1$ and $Pd2$ can be performed using a coordinate rotation, results are shown in Eq. (42) with example of Pa in Eq. (43).

$$P = \int_{\min_{x2}}^{\max_{x2}} \int_{\min_{x1}}^{\max_{x1}} p1(\xi_1, \mu_1, \sigma_1) p2(\xi_1 - \xi_2, \mu_2, \sigma_2) d\xi_1 d\xi_2 \tag{42}$$

$$Pv1 = \int_{dsml}^{-dsml} \int_{dsaf}^{\infty} p1(\xi_1, \mu_1, \sigma_1) p2(\xi_1 - \xi_2, \mu_2, \sigma_2) d\xi_1 d\xi_2. \tag{43}$$

The remaining probability of not detecting a specification violation is summarized in parameter P_{ndet} of Eq. (44).

$$P_{ndet} = Pv1 + Pv2. \tag{44}$$

2.4. Sensor system optimization considering signal comparing safety mechanisms

In safety critical applications, it is necessary to know the reliability and possible faults in sensor systems. On way to judge sensor data is shown in Ref. [18]. In two channel redundant sensor setups, two independent sensor signal paths are used for measurement of the desired signal by averaging and additionally use the two channels for signal comparison (see Fig. 9). This case was analyzed in a separated publication [19]. Fig. 10 shows the joint probability density function including combined averaged safety limit ($dsaf$) and diagnostic limit ($dsml$). Here, one can also recognize the areas $Pv1$ and $Pv2$ where the difference comparison will not detect this safety-limit violation and leads to a reduction of diagnostic coverage. One can also see regions $Pd1$ and $Pd2$ where a false-alarm is generated but no violation of safety-

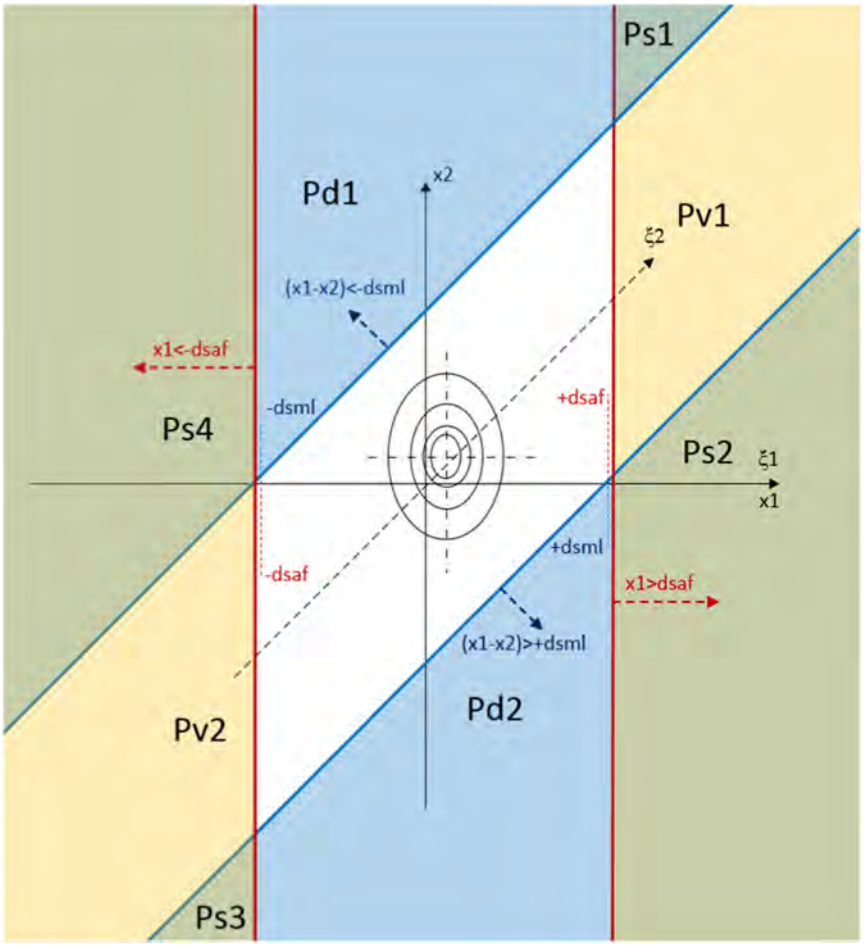

Fig. 8. Joint probability density function of tested sensor system acc. Fig. 7 with measurement output errors shown on $x1$ and reference sensor channel errors shown on $x2$. Red lines show the specification-limit and the blue lines show the detection limit. (For interpretation of the references to color in this figure legend, the reader is referred to the web version of this article.)

limit is present.

The calculation of sensor system probability providing data in regions *Pv*1, *Pv*2, *Pd*1 and *Pd*2 can be calculated using a coordinate-rotation as shown in Eq. (45) with an example shown in Eq. (46).

$$P = 2\int_{\min_{x2}}^{\max_{x2}}\int_{\min_{x1}}^{\max_{x1}} p1(\xi_1-\xi_2,\mu_1,\sigma_1)\cdot p2(\xi_1+\xi_2,\mu_2,\sigma_2)d\xi_1 d\xi_2 \tag{45}$$

$$Pv1 = 2\int_{-\frac{dsml}{2}}^{\frac{dsml}{2}}\int_{dsaf}^{\infty} p1(\xi_1-\xi_2,\mu_1,\sigma_1)\cdot p2(\xi_1+\xi_2,\mu_2,\sigma_2)d\xi_1 d\xi_2. \tag{46}$$

3. Implementations and results

3.1. Sensor system optimization implementation using statistical methods

3.1.1. Optimization of magnetic field based angular sensors

A further example of sensor optimization applying statistical optimization methodologies is shown in Ref. [20]. Here, magnetic field based angular-sensor optimization was performed using the Fisher Information. Magnetic field based angular sensing is done using Hall elements or magnetoresistive elements (see Fig. 11). In general sinusoidal components of the magnetic field caused by the rotation of a diametral magnetized magnet is measured according Eq. (47) and the mechanical angle is calculated using trigonometric functions via generation of sine and cosine components out of individual measured field values shown in Eq. (48).

$$S(\theta) = A\cdot\sin(\theta-\varphi)+w \tag{47}$$

$$\hat{\theta} = a\tan\left(\frac{\sin(\hat{\theta})}{\cos(\hat{\theta})}\right) = a\tan\left(\frac{f(S_i(\theta,\varphi))}{g(S_i(\theta,\varphi))}\right) \tag{48}$$

where functions $f(\cdot)$ represents the calculation of the sine-component and $g(\cdot)$ the cosine-component out of individual sensor values S_i, θ the relative angular position, A the amplitude and φ a phase shift linked to the sensor location/orientation (compare with Ref. [21]). The term w summarizes random deviations and noise.

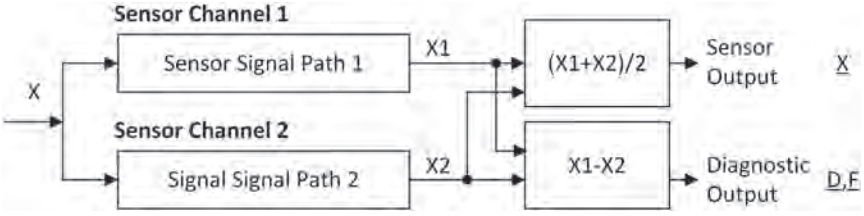

Fig. 9. Redundant sensor system block diagram with two signal paths where both sensor outputs contribute to the measurement output as well as to the safety-mechanism by comparison.

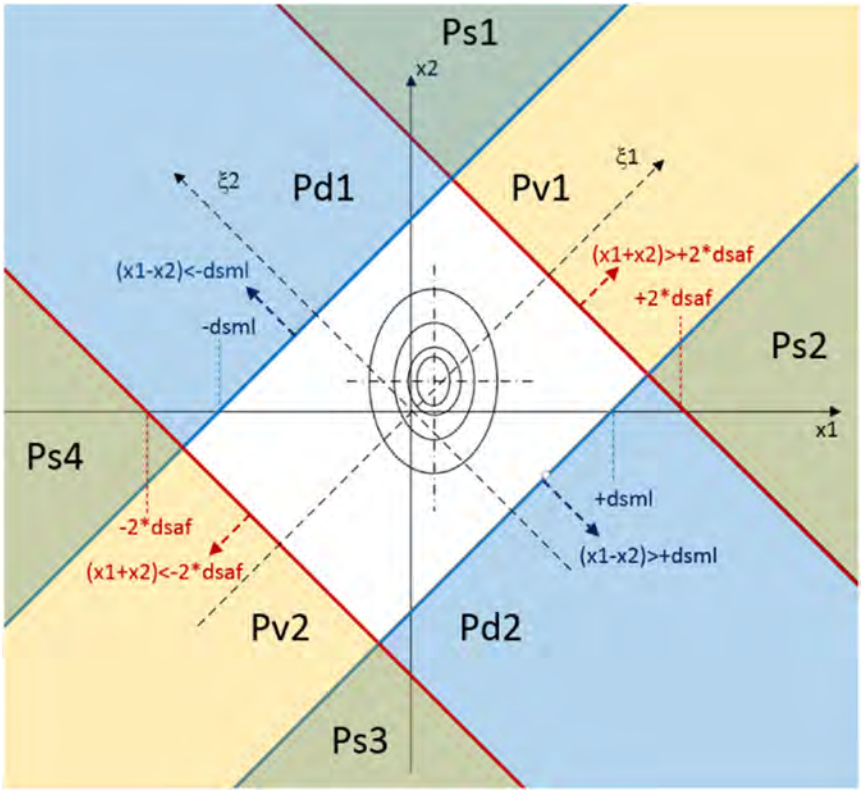

Fig. 10. Joint Probability Density function of a redundant sensor system acc. Fig. 9 with measurement output errors shown on $x1$ and redundant sensor channel errors shown on $x2$. Red lines show the safety limit and the blue lines show the diagnostic mechanism limit. (For interpretation of the references to color in this figure legend, the reader is referred to the web version of this article.)

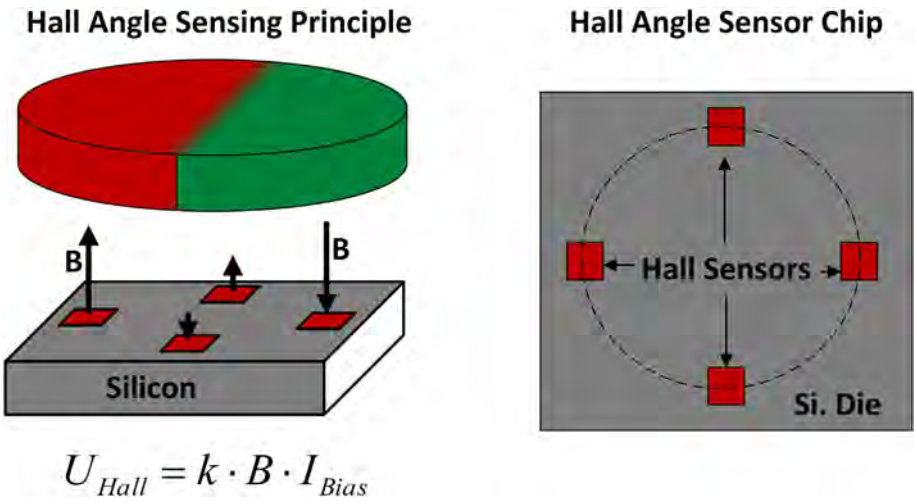

Fig. 11. Integrated Hall angle sensing principle. Several lateral Hall sensors are placed around a circle to measure the angle dependent magnetic filed in z-direction of a diametral magnetized rotating magnet.

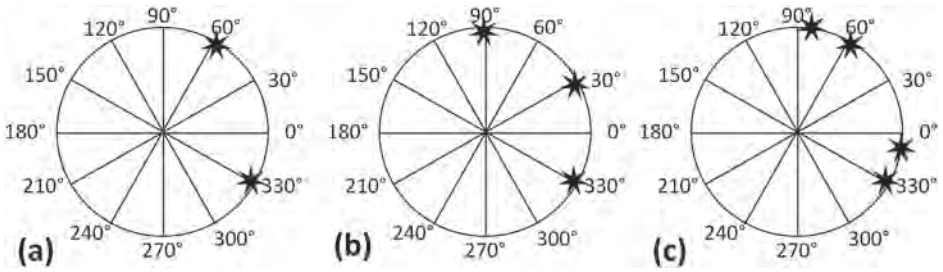

Fig. 12. (a) Two sensors: the optimal solution is found for a phase difference of 90°; (b)Three sensors: phase differences of 60° and 120° are optimal; (c) Four sensors: two pairs of 90° phase shift are found to be optimal, however the phase between the pairs is arbitrary.

Table 1
Results of different sensor-configurations in different deviation-models.

Configuration	Model	90° uniform
Two sensor elements	Uncorrelated	Yes
	Common offset	Yes
	Correlated	No
More sensor elements	Uncorrelated	Yes, not unique
	Common offset	Yes
	Correlated	Yes

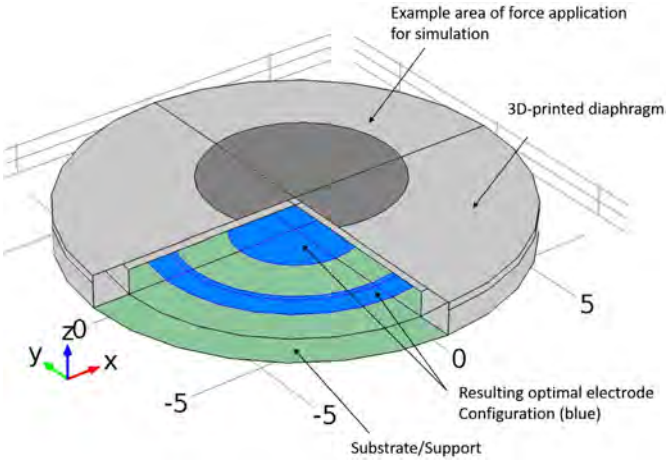

Fig. 13. Schematic of the pressure sensing system. The nominal action of the force is at the center of the diaphragm, in normal direction of the diaphragm plane, with several concentric capacitive sensing electrodes on PCB side.

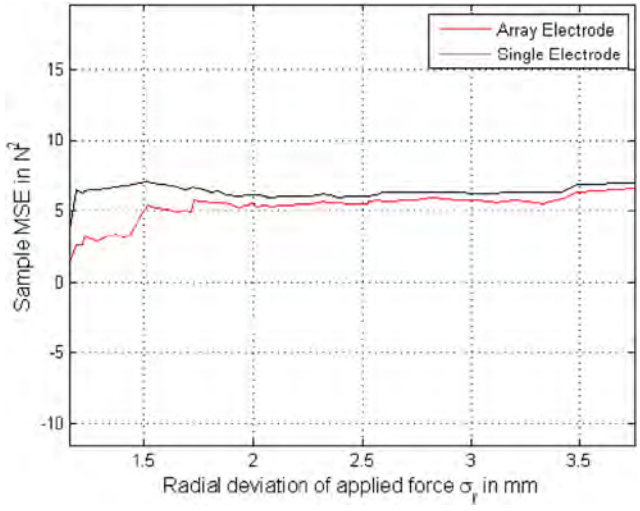

Fig. 14. This graph shows the Mean Square Error (MSE) of radial deviations from the center where a force is applied. The MSE is reduced with increased number of electrodes.

In real implementations the measurement vector $S(\theta)$ also depends on geometric properties η so that we can express Eq. (47) into Eq. (49).

$$S(\theta, \eta) = A \cdot \sin(\theta - \varphi(\eta)) + w. \tag{49}$$

The model described by Eq. (49) can be rewritten by splitting angle contributions into orthogonal in-phase and quadrature components according Eq. (50).

$$S(\theta, \eta) = I_A(\theta, \eta) \cdot \cos(\varphi(\eta)) + Q_A(\theta, \eta) \cdot \sin(\varphi(\eta)) + w \tag{50}$$

$$S(\theta, \eta) = H(\eta) \begin{bmatrix} I_A \\ Q_A \end{bmatrix} + w = H(\eta)\theta + w. \tag{51}$$

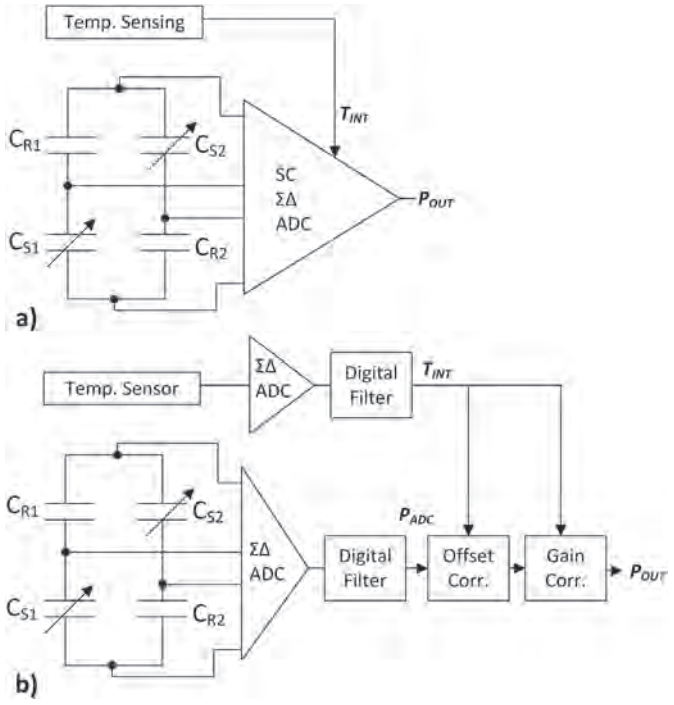

Fig. 15. The pressure signal is transferred into a differential voltage and converted into the digital domain by a switched capacitorΣΔ -ADC. Also the temperature is measured and used for analog temperature offset and gain correction. In a) the temperature compensation is done analog [32] and in b) in the digital domain [31].

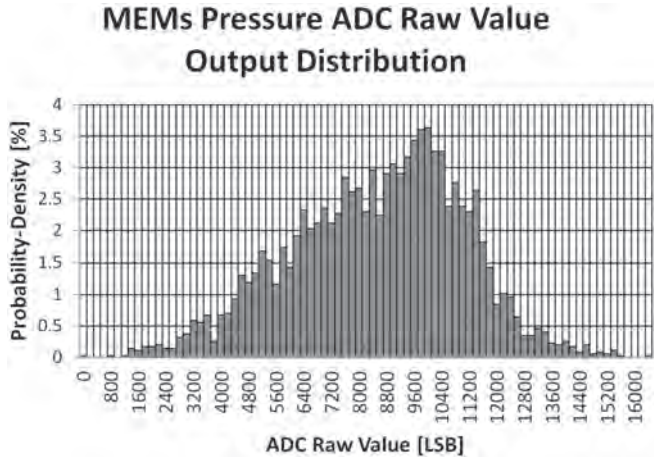

Fig. 16. MEMS pressure sensor ADC raw signals probability density at ambient air pressure and room temperature.

Different scenarios have been studied. Fig. 12 shows solutions for the uncorrelated case. For two sensor elements, a phase shift of 90° is obtained; for three sensors, a phase shift of 60°, as expected. However, for four sensors, a phase shift of 90° between all magnetic field sensors is not a unique optimum solution; any solution where two sensors in pairs are separated by 90° is also optimal. If we look at the objective function, it turns out that there is not a unique solution even in the case of three sensors. However, if we introduce a random common offset to the sensor elements, the objective function changes significantly. The solution with a phase shift of 120° remains, the objective function has two peaks, but the solutions are equivalent. When we increase the number of sensors, it turns out that we obtain a uniform distribution of the sensors when the I/Q approach is used (Table 1).

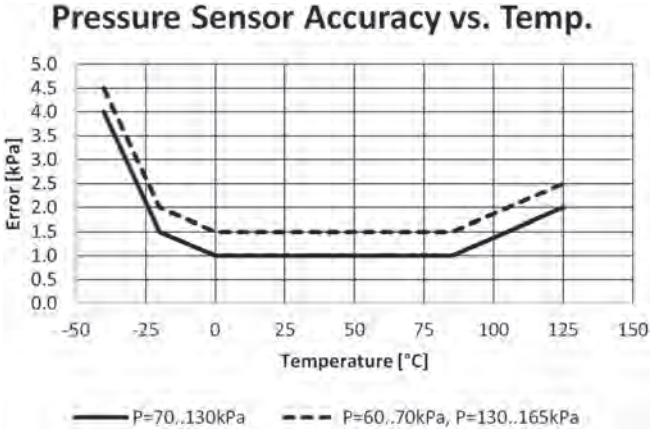

Fig. 17. MEMS pressure sensor performance, error versus temperature. For this pressure sensor, two different accuracy-ranges for two different pressure ranges are defined.

3.1.2. 3D-printed force /pressure sensors

Sensing of pressure and/or force is an important topic with versatile application areas. Capacitive sensing enables high resolution sensing in combination with high bandwidth and excellent linearity. Furthermore, the capacitive technology offers production related advantages such as low-cost designs with basic structures being readily manufactured with printing processes. 3D-printing technologies improved in the last decade and lead to production possibility of 3D-printed pressure sensors. Despite the advantages for rapid prototyping, both printing processes suffer from tolerances in excess of those from standard processes such as deposition or Printed Circuit Board (PCB) fabrication. It is thus mandatory to evaluate design criteria with respect to variations in topology (size, accurate positioning) as well as boundary conditions (uniform pressure vs. force on differing areas and locations) and material properties (conductivity, linearity, deformation hysteresis). In Ref. [22], Finite Element Model (FEM) simulations of the capacitive device are structured following a Design Of Computer Experiments (DOCE) targeted at determining an optimal calibration process for the considered sensor structure. The novelty lies in the suggestion to employ DOCEs and statistical signal processing in a dedicated way, combining beneficial properties of both, leading to an overall robust sensor design. The whole system is comprised of a circular 3D-printed steel diaphragm superposed to an inkjet-printed electrode structure. The axially symmetric design is supposed to be advantageous with respect to geometrical variations such as rotation. The steel diaphragm is depicted and an illustration of how the measurand (here: force) should ideally act on the topology including electrode geometries is given in Fig. 13. The bottom electrode is used as transmitter while the steel housing incorporates the receiver and are assumed to form a structure resembling a parallel plate capacitor describable by the simplified model described by Eq. (52).

$$\Delta C = \frac{\epsilon_0 \epsilon_r A_r}{\Delta d}. \tag{52}$$

ΔC is the change in capacitance in farads, A_r the active plate area in square meters, e_0 the dielectric constant of vacuum, e_r the relative dielectric constant of the material between the plates and d the plate spacing in meters. There self-capacitance measurement mode [23] was used which offers better SNR than a differential system, and disregard environmental influences due to the closed system setup (compare [24]).

In Ref. [25] a segmented electrode structure was proposed and optimization of design parameters (here geometric parameters) of the electrodes were performed. The optimization results in reduced Mean Square Error (MSE) compared to usage of one single electrode (see Fig. 14).

In Ref. [26], a similar setup was used and there the influence of prestress in the design of a capacitive force/pressure sensor was analyzed. Finite Element Model (FEM) simulations of this force/pressure sensor setup as shown in Fig. 13 were performed including prestress loading.

For the analysis of the topology and material variations of the target capacitive sensor, so-called Response-Surface-Methods (RSM) (see e.g. Refs.[27, 28]), specifically Central Composite Designs (CCDs) and Box-Behnken (BB) Designs are employed. These designs allow to describe the response over the simulated region as quadratic function of the design variables. The CCD is chosen as so-called *faced* design (CCF). This type of design restricts the levels for the design parameters in a way that there are no points outside the region of interest. The BB design is often employed due to the lower number of runs required. A drawback of BB designs is less accuracy in the extremal points, since these are avoided in the experiments. Subsequently, ANalysis Of VAriance (ANOVA) was performed of the gathered simulation results and the significance of design parameters influences and their interactions is determined. The significance is evaluated through hypothesis testing, yielding two well-known statistical measures: the *F*- and *t-statistics*.

The noise variables, i.e. varying material parameters are included as nested design. They are sampled from a normal distribution with mean μ and standard deviation σ_d as given. The standard deviation of noise variables is taken as specified by the manufacturer [29].

3.2. Sensor system optimization implementation by dependent parameter compensation

The optimization by dependent parameter compensation can be separate by the number of dependent parameters to compensate.

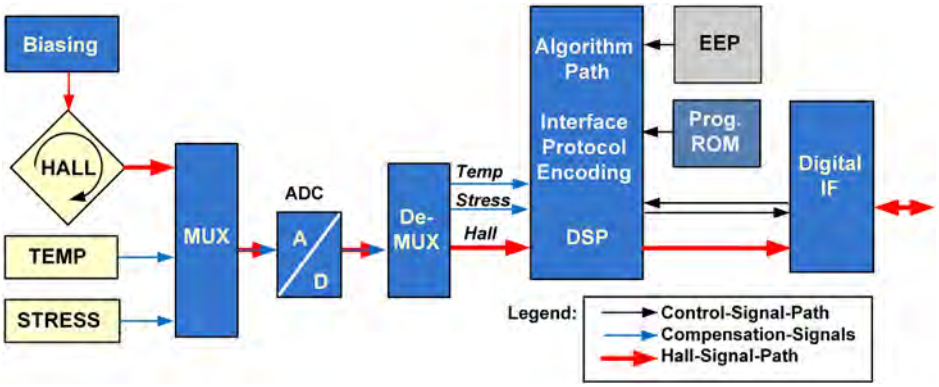

Fig. 18. Magnetic field Hall sensor system concept block diagram with temperature and stress measurement including compensation in the digital signal processor (DSP).

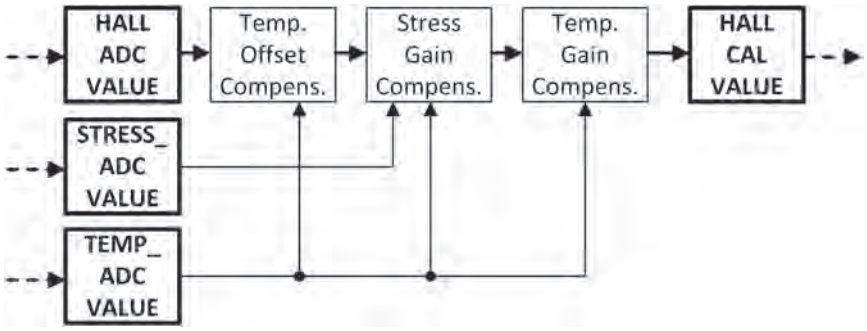

Fig. 19. Magnetic field Hall sensor system algorithmic datapath. Here, one can see the algorithmic block diagram of this digital temperature and stress-compensation of the Hall sensor magnetic field signal.

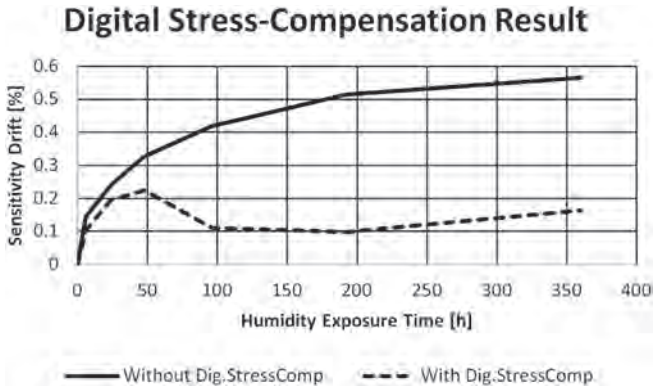

Fig. 20. This is the improvement of Hall-sensor sensitivity-drift by additional digital stress gain-compensation. These tests were done by placing the samples into a water-tap between readouts to increase the moisture-content and change the package-stress.

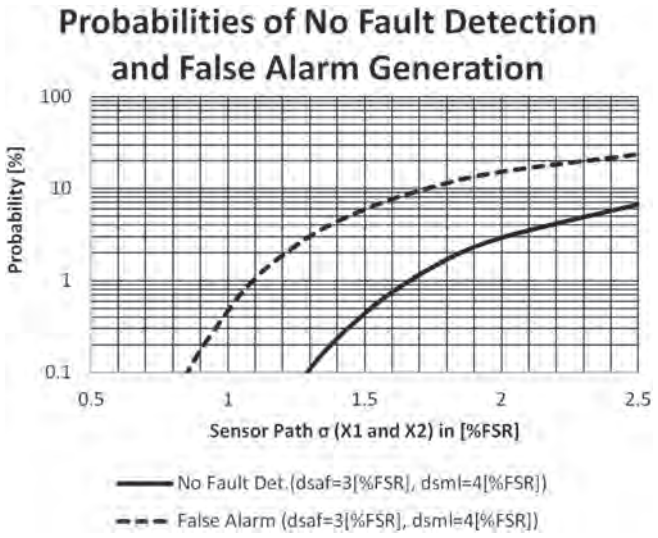

Fig. 21. Probability of safety-criteria violation and false alarm generation caused by measurement uncertainty. Here, a sweep of measurement uncertainty was analyzed from 0.5 [%FSR] to 2.5 [%FSR].

3.2.1. Single influencing parameter compensation

Many available measurement systems additionally measure one additional dependent parameter for compensation of this effect. The most famous parameter is the temperature which influences nearly all types of sensor elements. Luckily the temperature can be measured relatively simple in integrated sensor systems. Some examples of temperature compensation can be found in magnetic field Hall sensors [2], magnetoresistive sensors [30] as well as Micro-Electro-Mechanical System (MEMS) sensors [31-33]. An interesting implementation of accurate temperature measurement is shown in Ref. [34], where a very accurate temperature measurement can be achieved via an accurate voltage reference only.

As a temperature compensation example these MEMS pressure sensors system [31] and [32] were chosen. A specially developed capacitive ΣΔ-ADC converts the resulting bridge output-capacitances amplified into a digital signal (see Fig. 15). Since the temperature has a significant influence to the MEMS performance also the temperature is measured and transferred into the digital domain by a ΣΔ-ADC for further digital temperature compensation by one of these concepts. The ADC raw signals of this capacitive MEMS based pressure sensor can be seen in Fig. 16, which shows a significant spread and temperature dependence. This internal temperature signal T_{int} extracted from the temperature dependent bandgap voltage was used to compensate temperature related deviations of this MEMS pressure sensor according Eq. 53, where P_{off} represent the pressure offset-value which is temperature compensated via the internal temperature signal T_{int} and a certain offset temperature coefficient *TCO*. Also, the multiplicative correction factor amplitude or also called gain P_{Gain} is temperature compensated in the same way via a gain temperature coefficient *TCG*.

$$P_{out} = (P_{ADC} + P_{Off}(1 + TCO \cdot T_{int})) \cdot P_{Gain}(1 + TCG \cdot T_{int}). \quad (53)$$

Finally, this system achieves temperature dependent performance even within lifetime shown in Fig. 17

3.2.2. Compensation of two dependent parameters

To further increase sensor precision, several sensor systems measure two infuencing parameters and use them for compensation of their deviating influences. This results in more sophisticated productive calibration but can still be handled. Famous examples there are Hall based magnetic field sensors. It was recognized that beside the temperature dependence there also exits a varying mechanical stress in chip-packages [35] which influences Hall sensitivities [36, 3]. Most of high performance integrated Hall sensor system manufacturers use this temperature and stress compensation inside their integrated systems [37-39] and [40].

As an example for two parameter compensation [40] was chosen where the magnetic field, temperature and stress signal are transferred into the digital domain for further digital error-compensation in a digital signal processor (DSP). The block diagram of one such Hall sensing channel can be seen in Fig. 18. A principle algorithmic datapath of this digital error compensation of temperature- and stress-effects of the Hall sensor magnetic field signal for such a measurement channel is shown in Fig. 19. Since temperature and stress effects of the Hall sensitivity shall be compensated, the temperature and stress sensors are located close to the Hall sensor elements. The mechanical chip stress changes with chip-package production, but can be compensated once in productive calibration. The chip stress also changes due to humidity-

change in the chip-package mold-compound. This effect cannot be eliminated by a one-time calibration procedure, instead the chip-stress must be measured and has to be used for Hall output signal gain-compensation. In Fig. 20 you can see the performance-improvement of a system described in Ref. [40] by on-chip digital stress compensation additionally to the implemented analog sensor-element stress-compensation via the biasing.

3.3. Sensor system optimization implementation for safety critical applications

An implementation of a two channel redundant magnetic field sensor system with signal comparison for safety critical applications was shown in Ref. [40].

The probability to violate the safety criteria or to generate a false alarm caused by plain measurement uncertainty can be seen in Fig. 21, where the measurement uncertainty was swept in the useful range and data are calculated for two different combinations of a safety-limit (*dsaf*) and a diagnostic limit (*dsml*). All data are expressed in % of full-scale-range of the measurement system [*%FSR*]. The probability of safety-violation detection is called *Diagnostic Coverage* (DC) and calculated acc. Eq. (54) whereas the probability of a detection of a *False-Alarm* (FA) is calculated acc. Eq. (55). Here, it can be seen that with decreasing diagnostic limit (*dsml*) the diagnostic coverage increases but also the false-alarm-rate increases.

$$DC = 1 - Pv1 - Pv2 \tag{54}$$

$$FA = Pd1 - Pd2. \tag{55}$$

4. Conclusion

In this work, we showed several possibilities to reduce measurement uncertainties to fulfill reliability requirements. This can be done by statistical methods applying optimal design of experiment methodologies. Statistical optimizations benefit from the fact that we do not need to measure the influencing parameter but design the sensor system in a way that external influencing parameters have lowest possible effects. In case of further reducing the uncertainties correlations of influencing parameters can be used. The compensation of influencing parameters can be done by measure them and use its values for reduction of their contribution to measurement uncertainties. It could also be shown how calibration and test uncertainties influence the sensor system in the same way as implemented sensor system uncertainties and need to be taken into account in the same way when optimizing sensor systems. Additionally optimizations of reliably working safety mechanisms of safety critical sensor systems can be performed using the statistical considerations of calculating probabilities for not detecting a fault as well as raising false alarms. These reduced uncertainties increase the reliability of these sensor systems to fulfill all the required specifications.

Acknowledgments

This project has received funding from the Electronic Component Systems for European Leadership Joint Undertaking under grant agreement No 692480 (IoSense). This Joint Undertaking receives support from the European Unions Horizon 2020 research and innovation programme and Germany, Netherlands, Spain, Austria, Belgium, Slovakia.

References

[1] S. Kay, Fundamentals of Statistical Signal Processing: Estimation Theory, Prentice Hall, New Jersey, 1993.
[2] L. Giorgi, Sensitivity calibration and test of a 3D Hall integrated sensor device with an external magnetic field source on a new ATE concept, 20th International Mixed-Signal Testing Workshop, 2015, p. 1.
[3] M. Motz, U. Ausserlechner, Electrical Compensation of Mechanical Stress Drift in Precision Analog Circuits, Wideband Continuous ΣΔ ADCs, Automotive Electronics and Power Management, Chapter 16, Springer International, 2017, pp. 297–325.
[4] ISO 26262: Functional Safety on Road Vehicles 2011.
[5] JCGM 100:2008 Guide to the expression of uncertainty in measurement 2008.
[6] JESD88E: Dictionary of Terms for Solid State technology 2013.
[7] JEP70C: Guide to Standards and Publications Relating to Quality and Reliability of Electronic Hardware 2013.
[8] A.E. Council, AEC-Q100: Failure Mechanism Based Stress Test Qualifcation for Intergrated CircuitsAECQ-100 Rev-H 2014.
[9] I. of Electrical, E. Engineers, IEEE 1332-1998: IEEE Standard Reliability Program for the Development and Production of Electronic Systems and Equipment 1998.
[10] I.E. Commission, IEC TC 56: Dependability 1992.
[11] JESD99C: Terms, Definitions, and Letter Symbols for Microelectronic Devices 2012.
[12] E. Ryan, C.C. Drovandi, J.M. McGee, A.N. Pettitt, A Review of Modern Computational Algorithms for Bayesian Optimal Design. Int. Stat. Rev. (2016) 128–154, http://dx.doi.org/10.1111/insr.12107.
[13] V. Fedorov, P. Hackl, Model-Oriented Design of Experiments, in: P. Bickel, P. Diggle, S. Fienberg, K. Krickeberg, I. Olkin, N. Wermuth, S. Zeger (Eds.), Vol. 125 of Lecture Notes in Statistics, Springer, NY, USA, 1997, , http://dx.doi.org/10.2307/1271005.
[14] H. Zangl, G. Steiner, Optimal Design of Multi-parameter Multi-sensor Systems, IEEE Trans. Instrum. Meas. 57 (2008) 1484–1491.
[15] L. Liu, S. Wang, D. Liu, Y. Peng, Quantitative selection of sensor data based on improved permutation of entropy for system remaining useful life prediction, Microelectron. Reliab. 75 (2017) 264–270.
[16] C. Wang, L. Xiang, V.M. Vokkarane, Y. Sun, Reliability and lifetime modeling of wireless sensor nodes, Microelectron. Reliab. 54 (2014) 160–166.
[17] S. Askari, M. Nourani, An on chip sensor to measure and compensate static NBTI-induced degradation in analog circuits, Microelectron. Reliab. 53 (2013) 245–253.
[18] L. Liu, S. Wang, D. Liu, Y. Zhang, P. Yu, Entropy based sensor selection for condition monitoring and prognostics of aircraft engine, Microelectron. Reliab. 55 (2015) 2092–2096.
[19] W. Granig, D. Hammerschmidt, H. Zangl, Diagnostic Coverage Estimation Method for Optimization of Redundant Sensor Systems, IEEE Sensors Conference, 1 IEEESensors, Glasgow, UK, 2017, pp. 636–638.
[20] H. Zangl, L.-M. Faller, W. Granig, Optimal Design of Angular Position Sensors, COMPEL 36 (5) (2017) 1372–1385.
[21] U. Ausserlechner, The optimum layout for giant magneto-resistive angle sensors, IEEE Sensors J. 10 (2010) 1571–1582.
[22] L.-M. Faller, H. Zangl, Robust Design of a 3D- and Inkjet-Printed Capacitive Force/Pressure Sensor, IEEE Proceedings of the EuroSimE 2016, 2016.
[23] L. Baxter, Capacitive Sensors, Design and Applications, IEEE Press, 1997.
[24] L.M. Faller, T. Mitterer, J.P. Leitzke, H. Zangl, Design and Evaluation of a Fast, High-Resolution Sensor Evaluation Platform Applied to MEMS Position Sensing, IEEE Trans. Instrum. Meas. 67 (5) (2018) 1014–1027.
[25] L.-M. Faller, H. Zangl, Robust Design of an Inkjet-Printed Capacitive Sensor for Position Tracking of a MEMS-Mirror in a Michelson Interferometer Setup, Proc. of SPIE 10246, 2017.
[26] L.-M. Faller, H. Zangl, Considerations on Pre-Stress in a 3D-Printed Capacitive Force/Pressure Sensor, Proc. of EuroSimE, 2017.
[27] L. Wang, T.J. Kaymierski, B. Al-Hashimi, M. Aloufi, J. Wenniger, Response-Surface-Based DDesign Space Exploration and Optimisation of Wireless Sensor Nodes with Tunable Energy Harvesters, Desig, Automation & Test in Europe Conference & Exhibition (DATE) 2012, 2012.
[28] R.L. Mason, R.F. Gunst, J.L. Hess, Statistical Design and Analysis of Experiments, John Wiley & Sons, Hoboken, New Jersey, 2003.
[29] Feb, 2016, [link]. URL https://i.materialise.com/materials/high-detailed-stainless-steel/design-guide.
[30] W. Granig, M. Weinberger, C. Reidl, M. Bresch, M. Strasser, G. Pircher, Integrated GMR Angle Sensor for Electrical Commutated Motors including Features for Safety Critical Applications, Proceedings Eurosensors XXIV, 1 Eurosensors, Linz, Austria, 2012.
[31] C. Kolle, W. Scherr, D. Hammerschmidt, G. Pichler, M. Motz, B. Schaffer, B. Forster, U. Ausserlechner, Ultra Low-Power Monolithically Integrated Capacitive Pressure Sensor for Tire Pressure Monitoring, IEEE Sensors Proceedings, 1 IEEE Sensors, Vienna, Austria, 2004, pp. 244–247.
[32] C. Kolle, D. Maier-Schneider, A. Logiudice, R. Noe, E. Bodensdorfer, L. Gwehenberger, D. Draxlmayr, A Monolithically Integrated Capacitive Pressure Sensor System for Automotive Applications, Proc. fo 36th International Conference on Microelectronics, Devices and Materials 123-128, 1 MIDEM, Postojna, Slovenia, 2000.
[33] L. Wei, L. Kaiming, The intelligent compensation calibration algorithm for 3D polyhedron of the temperature drift of the silicon piezoresistive pressure sensor, IEEE internaltional conference on Electron Devices and Solid-State Circuits, Singapore, 2015, pp. 744–747.
[34] K. Souri, Y. Chae, K. Makinwa, A CMOS temperature sensor with a voltage-calibrated inaccuracy of ± 0.15°C (3σ) from −55 to 125°C, 2012 IEEE International Solid-State Circuits Conference, San Francisco, CA, 2012, pp. 208–210.
[35] A. Trigg, T.C. Chai, X. Zhang, X.T. Chen, L.C. Wai, Modular sensor chip design for package stress evaluation and reliability characterisation, Microelectron. Reliab. 52 (2012) 1581–1585.
[36] H. Husstedt, U. Ausserlechner, M. Kaltenbacher, In-situ analysis of deformation and mechanical stress of package silicon dies with an array of Hall plates, IEEE

Sensors J. 11 (2011) 2993–3000.
[37] S. Leroy, S. Rigert, A. Laville, A. Ajbl, G.F. Close, Integrated Hall-Based Magnetic Platform for Position Sensing, IEEE Eusopean Solid State Circuits Conference, Leuven, Belgium, 2017, pp. 360–363.
[38] M. Motz, U. Ausserlechner, W. Scherr, B. Schaffer, An Integrated Magnetic Sensor with Two Continuous-Time ΔΣ-Converters and Stress Compensation Capability, IEEE International Solid-State Circuits Conference, 2006.
[39] M. Motz, U. Ausserlechner, W. Scherr, E. Katzmaier, An Integrated Hall Sensor Platform Design for Position, Angle and Current Sensing, IEEE Sensors Conference, Daegu, Korea, 2006, pp. 1008–1011.
[40] W. Granig, F. Rasbornig, D. Hammerschmidt, M. Motz, T. Zettler, M. Strasser, A. Michelutti, Redundant and Diverse Magnetic Field Digital Linear Hall Sensor Concept for ASIL D Applications, SAE Technical Paper 2017-01-0053, 2017, http://dx.doi.org/10.4271/2017-01-0053.